Applied Energy 354 (2024) 122170

Contents lists available at ScienceDirect

Applied Energy

journal homepage: www.elsevier.com/locate/apenergy

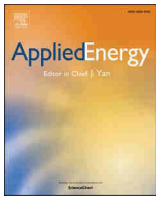

Hybrid storage system management for hybrid electric vehicles under real operating conditions

C. Beatrice [a], C. Capasso [a,*], S. Doulgeris [b], Z. Samaras [b], O. Veneri [a]

[a] National Research Council of Italy - Institute of Sciences and Technologies for Sustainable Energy and Mobility, Naples 80125, Italy
[b] Laboratory of Applied Thermodynamics, Department of Mechanical Engineering, Aristotle University, Thessaloniki 54124, Greece

HIGHLIGHTS

- Energy management strategies for hybrid storage system are proposed for the case study of a commercial hybrid vehicle.
- Detailed vehicle and storage simulation models have been implemented in AVL CruiseM environment.
- Experimental activities are carried out to perform model parametrization and validation.
- The application and main advantages of the proposed strategies are evaluated for the vehicle running on RDE cycles.

ARTICLE INFO

Keywords:
Energy management strategies
Lithium-ion capacitors
Hybrid energy storage systems
Hybrid vehicles

ABSTRACT

This study proposes the use and management of hybrid storage systems to power hybrid electric vehicles with the aim of reducing the negative effects of high current values on battery cycling life. Findings derive from a case study on a commercial plug-in hybrid electric vehicle with battery pack operations supported by a Lithium-ion Capacitor module. Specific experimental laboratory activities focused on the parametrization and validation of an equivalent circuit model representing the behavior of Lithium-ion capacitors for integration into the overall vehicle model (designed calibrated and validated on the basis of data from on-board data acquisition and measurement systems). The simulation platform was used to test various energy management strategies for the hybrid storage system supplying the vehicle during real driving cycles characterized by different operating conditions and driving styles. Results highlight the benefits of using the considered management strategies in terms of battery durability, allowing performance comparison for different driving routes and styles.

1. Introduction

Hybrid Thermal-Electric Vehicles (HEVs) have been developed extensively since they are highly effective in reducing fuel consumption and CO_2 emissions with respect to conventional vehicles. Given this advantage, and supported by climate change mitigation policies, electrified vehicles are expected to become a major component of future vehicle fleets [1,2]. Although such vehicles also present advantages in overall vehicle efficiency, appropriate energy management strategies are required for optimal power sharing between on-board sources and energy storage systems.

The power demand from the electric drivetrain of hybrid road vehicles is generally highly variable, especially in urban areas with many rapid acceleration and deceleration phases. As reported in the literature [3,4], transient peak power operations negatively affect battery cycle life, thereby increasing overall vehicle maintenance costs. One possible solution is the use of electric double layer capacitors (EDLCs), which have shown encouraging benefits in automotive applications. In particular, the combined use of supercapacitors and batteries in hybrid energy storage system configurations may increase the battery cycle life [5,6]. By reducing transient or peak currents, the use of EDLCs results in smoother battery current profiles [7].

However, with specific reference to the automotive sector, recent EDLC technologies are still characterized by poor performance in terms of specific energy, and they increase the overall vehicle weight. For these reasons, over the years their use has been mainly limited to railway and heavy-duty applications. In an attempt to overcome EDLC energy density issues, the use of Lithium Ion Capacitors (LICs) in hybrid energy

* Corresponding author.
E-mail address: clemente.capasso@stems.cnr.it (C. Capasso).

https://doi.org/10.1016/j.apenergy.2023.122170
Received 29 July 2023; Received in revised form 26 September 2023; Accepted 23 October 2023
Available online 9 November 2023
0306-2619/© 2023 The Author(s). Published by Elsevier Ltd. This is an open access article under the CC BY-NC-ND license (http://creativecommons.org/licenses/by-nc-nd/4.0/).

storage systems for urban road vehicles has attracted increasing interest. The intermediate characteristics of LiC technology in terms of energy and power density bridge the gap between those of lithium batteries and EDLCs, overcoming on-board size and weight constraints. LiCs are created by using the anode of lithium-ion batteries and the cathode of EDLCs, with a lithium-ion salt solution in an organic electrolyte. The resulting energy density of the LiC is about 20 *Wh/kg* (much higher than that of EDLC but lower than that of lithium-ion batteries), with a power density like that of EDLCs. A complete overview and characterization of LiC cells can be found in [8], where authors also proposed the use of specific equivalent circuit models to simulate electric behavior of these kinds of devices. Recent scientific literature on LiCs focuses on active materials, which further increase the energy density [9]. In particular, remarkable improvements in the electric performance of lithium-ion capacitors, mainly in terms of power/energy density and cycling stability, have been observed by using combinations of carbon materials and binary metals [10].

The effectiveness of supercapacitor technologies and batteries in Hybrid Energy Storage Systems (HESSs) is strongly linked to the choice of an appropriate Energy Management Strategy (EMS). Much of the existing scientific literature proposes possible solutions for optimal power flow exchanges between on-board storage units. Comprehensive and updated reviews of those strategies can be found in the scientific literature [11], also in case of vehicles supplied by multiple on-board power sources [12,13]. In particular, Azizi et al. focus on load demand, proposing a strategy whereby DC bus voltage is regulated by both sources, depending on the needs of the load [14]. Ziyou Song et al. studied real-time EMSs for a hybrid energy storage system (HESS) with four logic controllers: a rule-based controller (RBC), a filtration-based controller (FBC), a model predictive controller (MPC) and a fuzzy logic controller (FLC) [15]. With reference to urban driving cycles, in which the use of supercapacitors coupled with hybrid Rechargeable Energy Storage System (RESS) is ideal because of the high dynamism, the main effect of hybridization is a considerable reduction in battery losses and therefore extension of the lifetime of expensive, normally short-lived batteries [16]. Golchoubian et al. [17] proposed a nonlinear model predictive control (NMPC) method as the energy management strategy for a battery-supercapacitor (SC) in a Toyota Rav4EV. Model Predictive Control (MPC) was also considered in [18], where the authors compared MPC, Fuzzy and dynamic programming techniques for real time management of a battery-supercapacitors hybrid energy storage system, in semi-active configuration, for an electric vehicle powertrain. The effectiveness of the proposed MPC strategy was also experimentally validated through a hardware-in-the-loop test platform. Zhang et al. [19] focused on a cost function to minimize the electricity consumption of the HESS and to optimize battery operation. Advisory dynamic programming (AD-DP) and Progressive Optimal Search were proposed in [20,21] for power management of a multi-source hybrid electric vehicle. In these cases, the formulation of an optimal control problem, in terms of situation-based solutions related to vehicle states, allowed significant reduction in computational efforts for real-time EMS applications. Wegmann et al. [22] proposed dynamic programming for optimal operation and a causal controller, which allows for a real-time applicable control of the system. Controller performance during three driving cycles was compared for two vehicle classes. Mesbahi et al. [23] analysed a management strategy based on particle swarm optimization, with the aim of minimizing battery power stress and improving its lifetime. Shen et al. [24] proposed a multi-objective formulation for optimizing the power split in order to enhance the battery lifetime and reduce HESS power losses. In this case dynamic programming was carried out to numerically solve the optimization problem for various drive cycle data sets. For an EV adopting HESS under real-life load fluctuations, Sun et al. [25] proposed a high-level algorithm to adaptively split the load between two sources and divert excess power into the SP via a smart power converter. In [26] Akar et al. proposed an EMS which not only regulates the UC state-of-charge but also smooths the battery power profile using a fuzzy logic controller and a rate limiter. Recent works also addressed optimal energy management problems through the use of deep neural networks (DNN) and reinforcement learning (RL). In this regard, in [27], DNN was used to train and predict the control parameters of HESS. Then a novel meta-heuristic algorithm called the Squirrel Search with Improved Food Storage (SS-IFS) Optimizer was used to generate the optimal controller parameters. Wang et al. [28] proposed an EMS based on a double-delay deep deterministic policy gradient for the case study of fuel cell/battery/supercapacitor powered electric vehicle. In this case, cost optimization problem, for f long-distance logistics trucks, was solved combining the Twin Delayed Deep Deterministic Policy Gradient (TD3) algorithm in deep reinforcement learning.

The above analysis highlights relevant interest of the scientific literature on mathematical and theoretical formulations of new EMSs, for different kinds of applications, characterized by relevant advantages for the battery durability and the overall vehicle efficiency. These evaluations are generally referred to the simulation of a vehicle powertrain operating under specific standard driving conditions. On the other hand, reliable simulations on such a complex system would require proper experimental validation activities, to be carried out both at single component level and for the overall system. In addition, although standard driving cycles can be considered as a good comparison tool for the measurement of exhaust emissions, they are generally far from vehicle actual operating conditions, which strongly depend on the specific driver style and road characteristics.

In this context, this paper proposes the implementation of an experimentally validated case study to evaluate and compare the performance of different EMSs for hybrid storage systems, composed of batteries and lithium-ion capacitors. The evaluations refer to a commercial hybrid vehicle running on Real Driving Emissions (RDE) cycles, acquired through specific measurement campaigns. The presented results highlight the advantage of using hybrid energy storage systems in terms of battery pack cycle life, by filling, at the same time, the research gap related to the lack of experimental knowledge about the actual behavior of components, vehicle and driver.

Main innovations and contributions of the proposed work can be synthesized as it follows:

1) experimental results coming from laboratory campaigns focused on the identification and validation of LiC simulation models;
2) validated vehicle simulation models and RDE Cycles, with different driving styles, obtained through experimental on-board measurement campaigns;
3) optimization and comparison of different energy management strategies, evaluated through the integration of LiC modules in a hybrid energy storage system to supply thermal-electric hybrid vehicle;

The results obtained from the simulations for different road and driving conditions highlight the advantage of using LiC-based hybrid energy storage systems in smoothing electric power required for the battery pack, with the related positive impact on its cycle life.

The rest of the paper is organized as follows. Section II presents the case study, considered for the evaluations reported in this paper, and describes the different strategies to be applied for the appropriate management of hybrid energy storage systems. Details on experimental activities for model parametrization and data acquisition are reported in Section III. Section IV presents the main findings and their discussion. The conclusions are reported in Section V.

2. Case study and energy management strategies

2.1. Case study

The evaluations reported in this paper mainly refer to the integration of a LiC module in HESS configuration with a validated vehicle

simulation model for a C-segment plug-in hybrid passenger car. The main vehicle specifications are reported in Table 1.

The considered vehicle is equipped with a 1.8 L internal combustion engine (ICE) and two electric machines (EMs), all connected through a planetary gearbox. The powertrain has a power-split architecture, which allows interaction between the ICE and the two EMs, ensuring optimal system efficiency. The main EM is connected directly to the wheels and is used mainly for propulsion or regenerative braking, whereas the second EM serves mainly as a generator. The ICE is connected to the wheels via the planetary gearbox and can provide power simultaneously to the EMs and the wheels. The gearbox is considered as an e-CVT, meaning that the ICE speed is controlled via the electric machine aiming to operate at the best possible efficiency point. The vehicle's powertrain is combined with a 25 Ah Lithium-ion high voltage battery with 352 V nominal voltage, which allows pure electric operation for 30–45 km under real-world driving conditions [29]. The powertrain layout of the vehicle along with the introduction of the LiC module is presented in Fig. 1. In the figure, the mechanical connections are illustrated with a black solid line and the electrical connections with a green dashed line.

The powertrain architecture of this vehicle allows energy to flow within all three components (the ICE and the two EMs), enabling several different operating modes for optimal system efficiency. The operating principle and layout of a vehicle with power-split powertrain architecture is described in Prati et al. [30]. The two main vehicle operating modes are pure electric driving or charge-depleting mode (CD) and hybrid operation or charge-sustaining mode (CS). Mode selection is made according to the high voltage battery's state of charge (SoC). When the battery is fully charged (SOC around 80%–85%), CD mode is enabled; when the SOC is low (12–15%), CS mode is enabled and the vehicle operates in hybrid mode. When operating in CD mode, the main EM is used to move the vehicle and cover the driver's power demand. However, during abrupt acceleration and high power demand, ICE is enabled and the operating mode shifts to hybrid. When operating in CS mode, the ICE and both EMs are activated and used to propel the vehicle. In CS mode, the battery is kept at a certain SOC that enables hybrid operation and prevents battery degradation due to extreme discharge. Fig. 2 illustrates schematically the logic diagram for the mode selection based on the battery state and the power demand.

The overall energy management strategy in the original thermal-electric hybrid configuration aimed to select optimal operating conditions for maximizing powertrain and ICE efficiency [31]. Fig. 3 shows the different operating points described, also including examples for pure electric driving and regenerative braking.

Fig. 3A presents the operation of the under two constant operating points and CS mode. During constant speed the two electric motors and the ICE work at the same point. From the energy balance it can be seen that the power flow of the high voltage battery is constant and close to zero, a favorable condition for the battery. However, this operation is not realistic operation, since during real world driving there is a more transient behavior. Fig. 3 B and C present the operation of the vehicle's powertrain under transient conditions of a real world velocity profile during CS mode. As it can be seen, within a small section of the cycle the vehicle passes through several operating conditions. That said, depending on the velocity and power demand there is a transition from hybrid driving with battery charging to regenerative braking and hybrid driving with torque assist (battery discharge) in less than a time internal of 100 s. This indicates that the high voltage battery is stressed with highly transient current. Fig. 3D shows the battery and electric motor power during CD mode. Although the operation seems less transient than in Figs. 3 B and C, since there is only transition from propulsion to regenerative braking, again the operation is far from the constant speed presented in Fig. 3A. As illustrated and commented in the time series presented in Fig. 3, several peaks in power occur during acceleration or regenerative braking when EMs operate in transient mode. Such peaks directly affect the high voltage battery, which should cover the power demand or absorb the electric energy from the EMs.

Table 1
Main vehicle specifications.

C-segment PHEV	
Engine	
Type	4 cylinder, Atkinson
Displacement & Fuel	1.8 L, Gasoline PFI
Max. Power	72 kW @ 5200 rpm
Body and powertrain	
Inertia weight	1470 kg
Transmission	e-CVT
Powertrain type	Power-split PHEV
Electric machine	
Max. Power	53 kW
High voltage battery	
Nominal capacity	25 Ah
Nominal Voltage	352 V

As already discussed in the introduction, the use of capacitor modules in hybrid storage configuration with the on-board battery pack greatly reduce the impact of high charging/discharging power demands on battery durability. In this case, a 125 *V* - 73 *F* lithium-ion capacitor module was used. The module consists of 44 cells connected in series with an overall module voltage of 96.8–167.2 *V*. The single LiC cell is an Ultimo 3300 F cell operating in the 2.2–3.8 *V* range. The main characteristics of the LiC cell are reported in Table 2.

A controlled DC/DC bidirectional power converter can be used to create a hybrid energy storage system by integrating capacitors and an on-board battery pack. A block diagram of the power architecture for the considered HESS, as well as the electric parameters, is reported in Fig. 4.

This configuration is generally referred as semi-passive (or semi-active) architecture, which represent a compromise among complexity, cost and performance of the overall hybrid energy storage systems. The configuration is based on the use of a single DC/DC power converter, interfacing super-capacitors with the battery pack, which are directly connected to the DC-Link of the electric drives. The use of the DC/DC converter enables the use of capacitor modules in their full voltage range and the control of power flows between capacitors and batteries on the basis of specific energy management strategies. More details and functional schemes about other possible configurations can be found in [32,33]. The considered EMSs are supposed to be controlled by means of the bidirectional DC/DC power converter, interfacing the battery pack and the LiC module so that the electric current required by the electric drives of the vehicle (on the DC side; I_{DC}) is split between them. This control is performed in current reference mode on the basis of the reference value of LiC current, I^*_{SC}.

2.2. Energy management strategies

This section presents three strategies for managing on-board power fluxes between the battery pack and the LiC module. These strategies, to be implemented using the control signals of the DC/DC power converter, are based on the input/output electric parameters of the DC/DC converter, vehicle speed and the rated capacitance of the LiC module. The strategies aim to reduce the effects of peak power demands (generated by driving cycles with fast transient dynamics) on the battery pack through the use of a LiC module. Therefore the performance of a single strategy can be quantified simply using the effectiveness parameter, as already proposed in previous works by some of the authors of this paper [34,35]. The effectiveness of a certain Energy Management Strategy, $Eff_{EMS}\ (T)$, can be evaluated taking into account battery durability losses in single, $L_{Batt}\ (T,)$ and hybrid storage configuration, $L_{HESS}\ (T)$, using the following two equations:

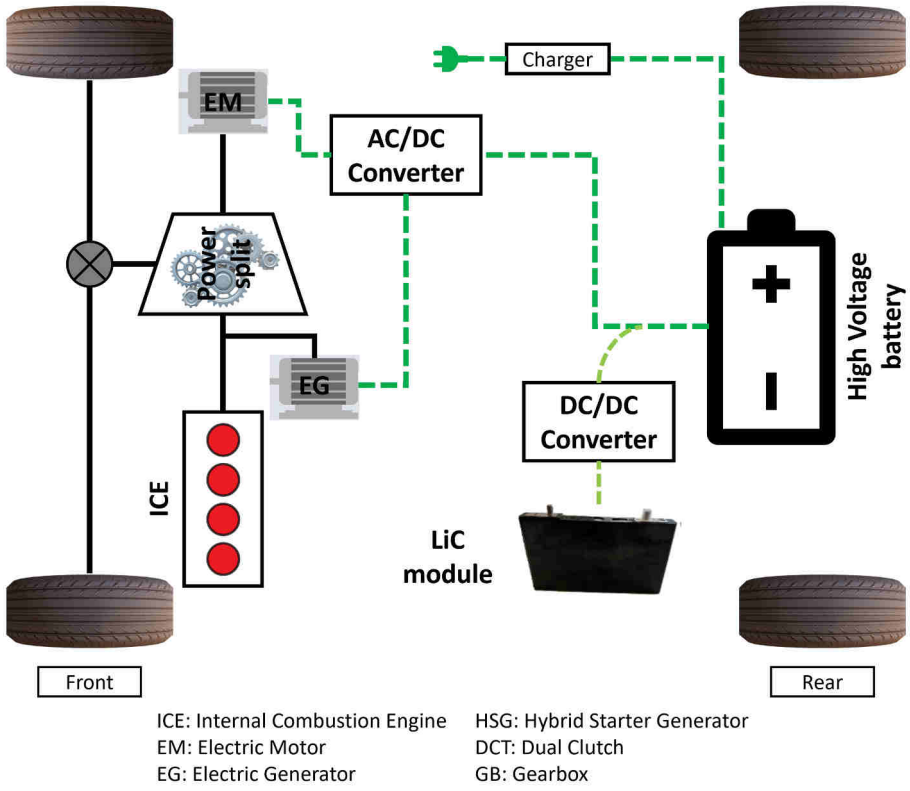

Fig. 1. Powertrain layout of the vehicle.

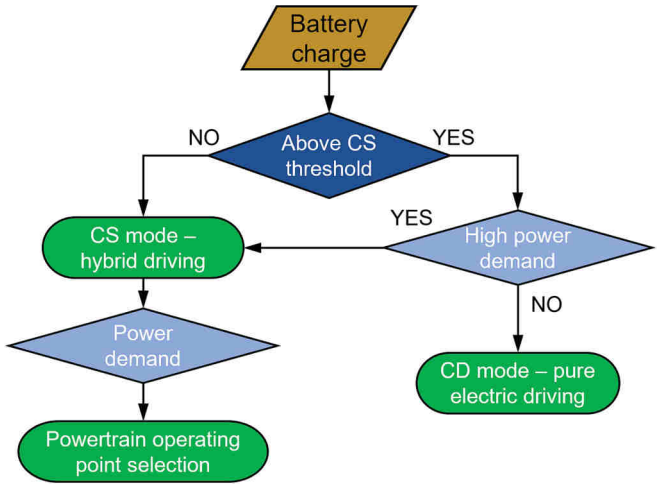

Fig. 2. Logic scheme for operative mode selection.

$$L\,(T) = \frac{1}{T}\int_0^T |I_{Batt}|^2 dt \tag{1}$$

$$Eff_{EMS}(T) = \frac{L_{Batt}(T) - L_{HESS}(T)}{L_{Batt\,j}(T)}. \tag{2}$$

where T is the duration of the working cycle.

All the considered strategies can work for real time on-board applications and are based on a common assumption regarding the management of vehicle regenerative braking operations and limitation of maximum LiC current values. As suggested in [36], during vehicle regenerative operations the battery pack receives electric power only when the LiC module is fully charged. This reduces battery pack usage by taking advantage of fast-charging LiCs. For the considered LiC module coupled with the related DC/DC bidirectional converter, the maximum current, I_{sc_max}, was set at 200 A. This value, when LiC voltage increases above the predefined low/high voltage threshold values, is linearly reduced to 0 A at the minimum/maximum voltage value. This control mode is generally implemented in DC/DC power converters to avoid sudden interruptions in high current values at LiC limit operating conditions.

The first considered strategy entails simply setting a DC current threshold value, I_{th}. Based on this value, the LiC module reference current under normal operating conditions is:

$$I^*_{SC} = \eta_{conv}\frac{V_{batt}}{V_{SC}}(I_{DC} - I_{th}). \tag{3}$$

This means that the considered threshold value limits the maximum battery current.

The second strategy involves the application of an Exponential Weighted Moving Average (EWMA) filter to the DC current demand of the electric drive, I_{DC}. Such filtering is generally used for control operations in energy storage systems with unpredictable power sources [37,38]. It can be used successfully in any application that combines high power and high energy devices. In particular, the EWMA for the i^{th} sample of the DC Link Current, $\bar{I_{DC,i}}$, can be calculated through the recursive evaluation of the following equation:

$$\bar{I_{DC,i}} = \lambda I_{DC,1} + (1-\lambda)\bar{I_{DC,i-1}}, \tag{4}$$

where λ is the decay factor, ranging from 0 to 1, which determines the weight assigned to instantaneous and previous EWMA results. As mentioned above, the main objective of EMSs is to smooth battery pack transient operations. The aim is to supply the EWMA of the DC Link Current, $\bar{I_{DC,i}}$, with the electric power from the battery pack, whereas the remaining amount of current can be supplied by the LiC module. The equation considers two consecutive time steps, consequently the simulation time step (set at 0.01 s) is also used as sampling time for the Eq. (4). The LiC module reference current under normal operating

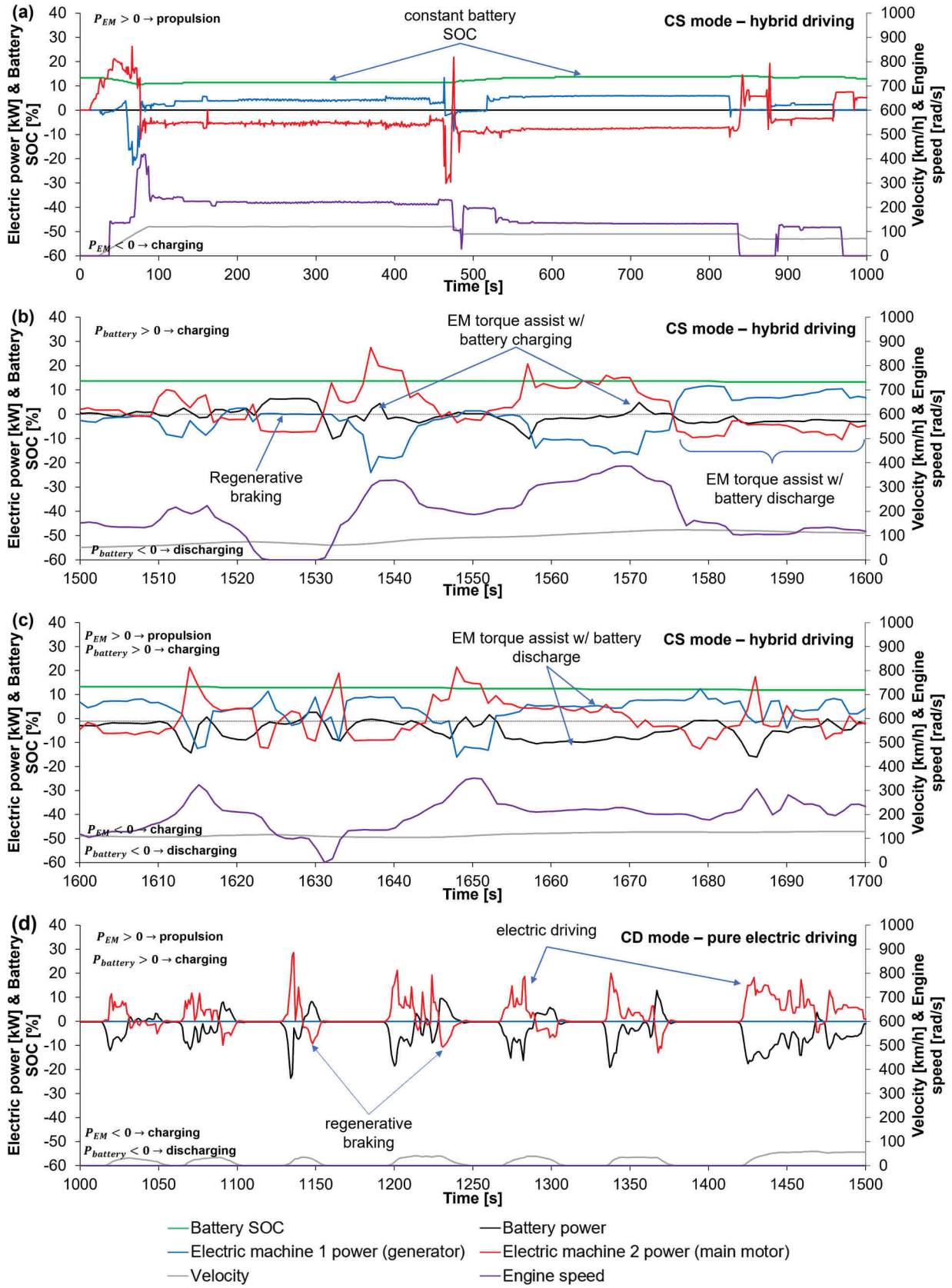

Fig. 3. Examples of vehicle operating points: (a) constant battery SOC and EMs operating as generator and motor, (b) battery charging with EM torque assist, (c) electric driving and regenerative braking.

Table 2
Main characteristics of the LiC cell.

Range of Operating Temperatures (K)	243÷343
Minimum Voltage (V)	2.2
Maximum Voltage (V)	3.8
Rated Capacitance (F)	3300
Weight *E*-density (Wh/kg)	15
Volume E-density (Wh/L)	20
Weight P-density (kW/kg)	10
Volume P-density (kW/L)	15
253 K Capacitance ratio (vs 298 K)	85%
343 K Capacitance ratio(vs 298 K)	100%
Single Cell size (mm)	150.0 × 93.0 × 15.5
Single Cell weight (kg)	0.365

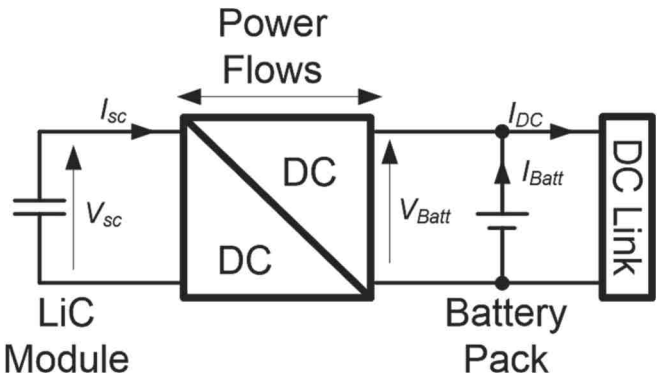

Fig. 4. Block diagram of the power architecture of the considered HESS.

conditions can be determined for each step through the following equation:

$$I^{*}_{SC,i} = \eta_{conv}\frac{V_{batt}}{V_{SC}}\left(I_{DC,i} - \bar{I}_{DC,i}\right). \tag{5}$$

The last strategy considered, herein referred to as the *power-based strategy,* is based on the following two main assumptions. The first is that peak power values for the electric drive are generally linked to the contribution of vehicle inertia during transient operations in each operating cycle. The second assumption is that the amount of power that can be stored/supplied during LiC module charging/discharging operations can be optimized by considering its overall operating voltage as a function of vehicle speed. The effects of the two contributions above can be directly applied to the battery pack side by determining the reference battery current value, I^{*}_{Batt}, which comprises two different terms. The first term, $I^{*'}_{Batt}$, is directly related to vehicle-road and aerodynamic resistant forces, which generally have low variability compared to fast transient operations involved by vehicle. This term is calculated as a function of mechanical resistant power, P_{res}, using the following equation.

$$I^{'*}_{Batt} = \eta_{el}\frac{P_{res}}{V_{DC}}, \tag{6}$$

where η_{el} is the overall efficiency of operative electric drives.

In calculating the second term, $I^{*''}_{Batt}$, it is assumed that to optimally smooth battery pack power, the LiC module should ideally receive/store all available vehicle kinetic energy during regenerative operations and supply all the energy required during peak power acceleration. The LiC module should ideally be fully discharged before regenerative operations and completely charged before peak power acceleration. On the basis of this assumption, under the hypotheses of linear dependence between LiC module voltage and its SoC, the reference LiC module voltage, V^{*}_{sc}, can be determined using the following equation, wherein the sum of the LiC module and vehicle kinetic energy equals a constant value, k.

$$\frac{1}{2}C\left(V^{*2}_{SC} - V^{2}_{min}\right) + \frac{1}{2}mv^{2}_{vehicle} = k. \tag{7}$$

In the equation above C represents the LiC module capacity, whereas values of k and V^{*}_{sc} as a function of vehicle speed, $v_{vehicle}$, can be easily calculated considering the module fully charged. V^{*}_{sc} therefore corresponds to the maximum allowed LiC module voltage when the vehicle speed is zero.

That value of V^{*}_{sc} represents an ideal LiC module voltage value to be tracked by the I^{*}_{sc} control system through the second term, $I^{*''}_{Batt}$. For the application considered herein, this second term is obtained using an additional PI controller, which compares the actual voltage of the LiC module, V_{SC}, to its reference value, V^{*}_{sc}. Consequently, the reference signal for the DC/DC converter current, I^{*}_{sc}, can be derived from the term, I^{*}_{batt}, which comes out from the block diagram reported in Fig. 5.

In this last strategy, effectiveness is strongly linked to vehicle speed and the high voltage battery's state of charge. Optimal parameters seem to differ for high and low initial SOCs, as well as for urban and rural driving. An adaptive strategy in which PI parameters changed dynamically was therefore applied. The SOC threshold for parameter adaptation due to battery SOC was set at 15%, whereas the velocity threshold was set at 60 km/h. With respect to constant PI values, adapting PI parameters enabled greater effectiveness (compared to the case of) under the same conditions.

For the vehicle considered in this case study, the above strategies were mainly compared in terms of effectiveness. This comparison was performed using an advanced, validated vehicle simulation model created with input from collected experimental data. In addition, a simulation environment was used to implement recursive procedures for optimizing the specific parameters (i.e. threshold values, λ and PI adaptive parameters) of all the considered strategies.

3. Modelling and data acquisition

3.1. LiC modelling

Capacitor modelling was performed at the single storage cell level. The resulting evaluations were then reported at the module level on the basis of electrical cell connections. Various kinds of approaches for modelling storage cells are proposed in the scientific literature (i.e. electrochemical, neural networks and equivalent circuit models). Models are characterized by different levels of precision and complexity. The Equivalent Circuit Model (ECM) adopted in this study was considered a good compromise between computational effort and accuracy.

The behavior of LiCs generally differs from that of classical electrical double-layered capacitors, since their open circuit voltage cannot always be considered a linear function of state of charge. Based on this consideration, the single capacitance-internal resistance model is clearly not suitable for modelling such devices. The considered equivalent circuit is therefore similar to the first order Thevenin circuit, a model generally proposed for lithium batteries [39,40], which is reported in Fig. 6.

The equations of the above equivalent circuit are:

$$V_{LiC} = OCV - R_0 I_{LiC} - V_1, \tag{7}$$

$$C_1\frac{dV_1}{dt} = I_{LiC} - \frac{V_1}{R_1} \tag{8}$$

In particular, the circuit is based on an ideal voltage generator, representing Open Circuit Voltage (*OCV*), a series resistance, R_0, representing the cell's internal resistance, and an R_1-C_1 branch representing the cell's dynamic response. All the considered parameters are a function of cell temperature and State of Charge (SoC).

Suitable experimental data is required to parametrize and validate the equivalent circuit model so as to accurately simulate cell behavior

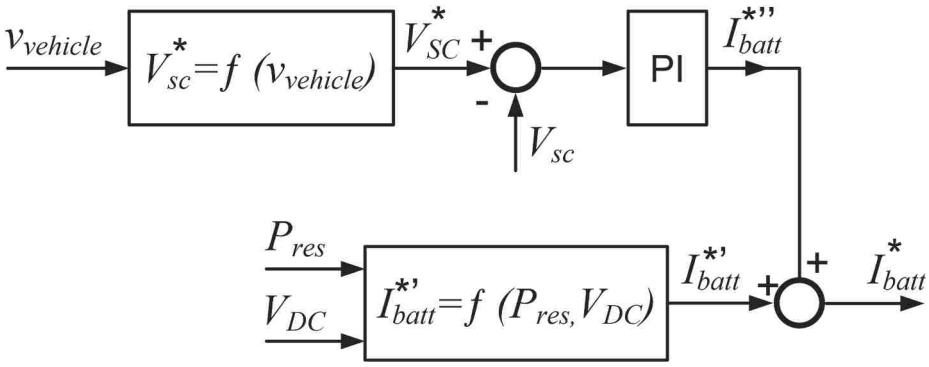

Fig. 5. Block diagram of the power-based strategy.

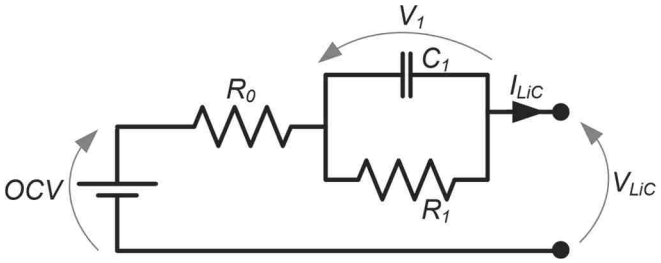

Fig. 6. Equivalent circuit model of the Lithium-Ion Capacitor cell.

under different operating conditions. Testing on LiC cells was performed in the CNR-STEMS laboratories in Naples. The experimental test bench for cell electric characterization activities consisted of a DC power supplier and a DC electronic load. These devices interfaced with each other through a master-slave communication interface, working together to perform charging/discharging cycles on the tested cell. The system was equipped with voltage, current and temperature sensors. All data were collected using a National Instruments cDaq acquisition device and stored in a remote PC. The acquisition and control software interface was installed on the remote PC and was programmed in the Labview environment.

As mentioned earlier, the behavior of the equivalent circuit parameters was also affected by cell temperature. All laboratory tests on the LiC cell were therefore performed at a constant temperature of 298 K. Constant temperature conditions were maintained using a 340 L climate chamber in which operative temperatures could be adjusted in the 233–453 K range. The experimental test bench with its main component is represented in Fig. 7.

Further details on the experimental test bench can be found in another paper by the same authors [41].

Before each test, the LiC cell was preliminary charged through CC-CV charging operations, with a maximum current value set at 10 A. After a 10-min resting period, the open-circuit voltage value corresponding to 100% SoC was evaluated.

After these preliminary procedures, the parametrization cycle, characterized by 100 A charging/discharging current pulses, was completed. This cycle is reported in Fig. 8 in terms of current versus time.

The considered cycle is composed of two 100 A current pulses lasting 4 s. After these pulses, a discharging operation at a constant 30 A current was performed to reach 10% SoC. After a ten-minute resting period, the open circuit voltage corresponding to the new SoC value was obtained. The cycle was repeated until the LiC cell reached its minimum voltage value of 2.2 V. Fig. 9 shows the behavior of cell voltage and current versus time for the considered cycle.

Based on the above cycle, with reference to the considered ECM, the value of R_0 can be derived by evaluating the sudden voltage drop/

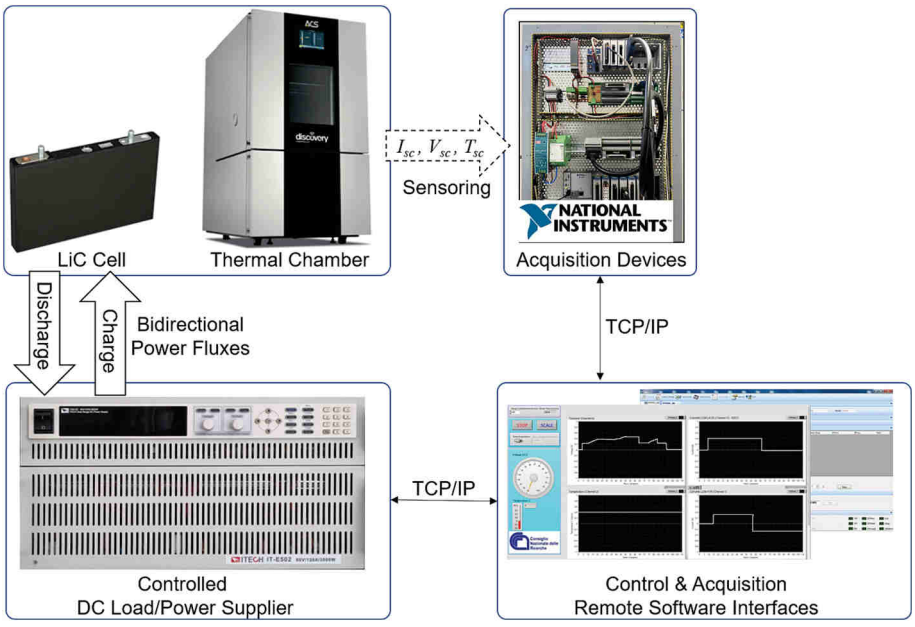

Fig. 7. Block diagram of the Experimental Test Bench.

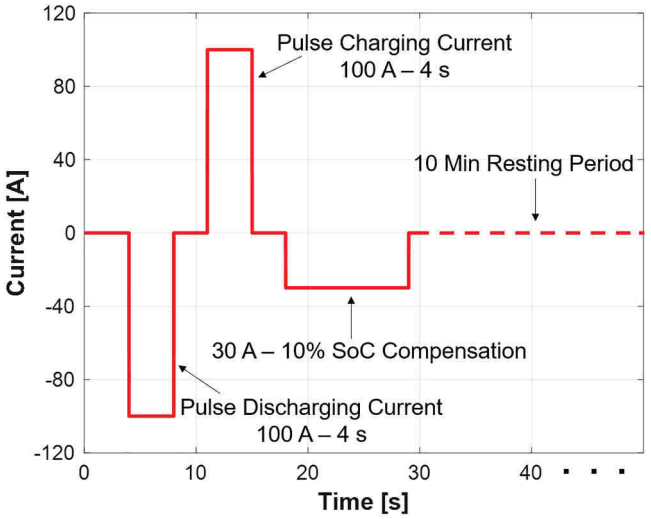

Fig. 8. Parameter identification cycle.

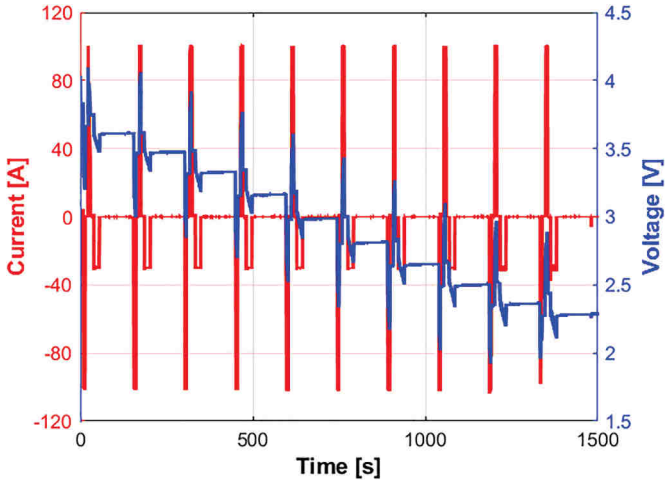

Fig. 9. Cell Current and Voltage behavior versus Time for the parameter identification cycle.

increase corresponding to the decrease/rising phase of current pulses. In a similar way, R_1-C_1 branch parameters can be evaluated by analyzing transient phases occurring immediately after zero-current conditions.

The above assessments were performed using the Matlab-Simulink parameter estimation tool, based on the minimization of the least square error between simulation and experimental data. The performance of the proposed ECM and of the resulting parameters, was evaluated on a validation cycle that obviously differs from the training cycle. In particular, the considered validation cycle is based on the Dynamic Stress Test (DST) profile proposed in [42]. The experimental behavior of the cell current in that cycle is reported in Fig. 10.

Fig. 11 A and B compare experimental and simulation results in terms of model Voltage response for the above current profile during the DST cycle. In particular, the obtained results highlight the model's good fit for the validation cycle, with an average and maximum residual voltage error of 0.009 and 0.05 V respectively.

The simulation model of the overall LiC module, for the case study considered in this paper, was obtained under the following simplifying hypotheses: additional resistances related to the electrical connections of the module cells were completely neglected; all the cells of the module were considered working in the same operative conditions in terms of temperature, state of health and state of charge. As a

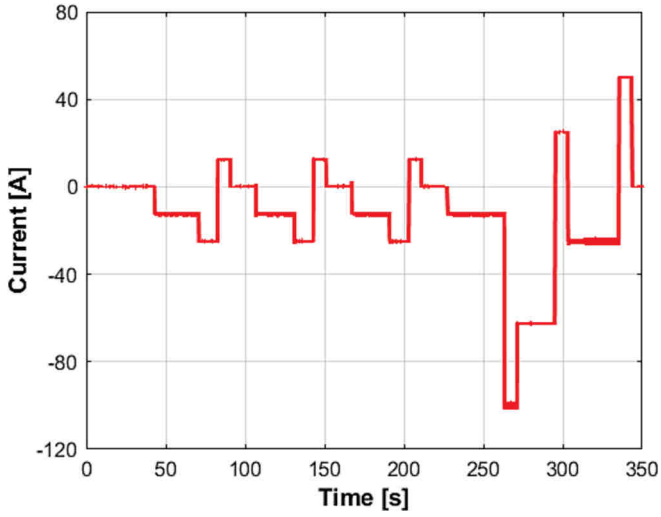

Fig. 10. Cell Current behavior versus Time for the DST validation cycle.

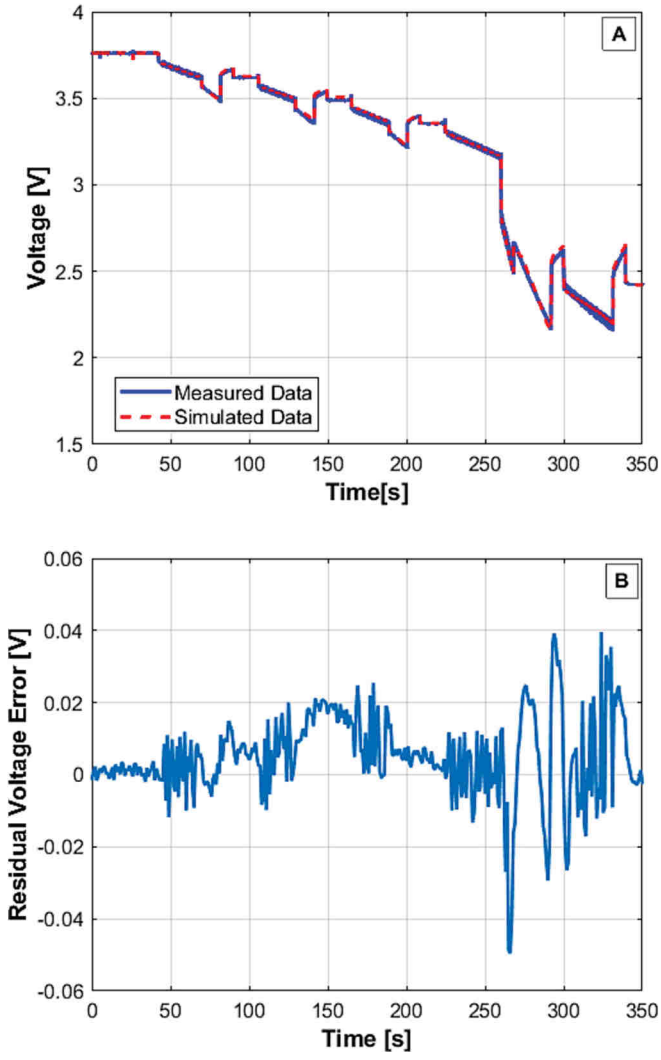

Fig. 11. Model performance analysis: Comparison between Experimental and Simulation data for cell voltage behavior versus Time (A) and Residual Voltage Error (B) during the DST validation cycle.

consequence, the simulation model of the LiC module has been obtained on the basis of the simple series connection of the cell equivalent circuits.

3.2. Vehicle modelling and RDE data acquisition

The simulation model used in this study was developed in the AVL CRUISE™ M simulation platform. The simulation model of the PHEV vehicle described in the previous section was modified by adding the LiC sub-model along with the energy Management Strategies. The overall layout of the model with the main sub-models, like the internal combustion engine, the electric machines, and the drivetrain components (planetary gearbox, final drive, wheels) is shown in Fig. 12.

In particular, the vehicle simulation model was developed according to the layout of the actual C-segment PHEV. A map-based simulation approach was used to simulate the ICE. The main input data for the ICE sub-model are the engine parameters (e.g. engine displacement, number of cylinders), the fuel consumption map, the full load and motoring curve, and fuel properties. Similarly, electric machines were simulated with a map-based sub-model in which an efficiency map and a full load curve are provided as input. The vehicle sub-model uses as input the Road Load (RL) or the vehicle characteristics (frontal area A, aerodynamic drag coefficient C_d, rolling resistance c_{roll}) and the mass (M_{veh}) of the simulated car, and for each velocity (v) point it calculates the tractive power (P_{trac}) at the wheels presented in Eq. (9) [43]. Velocity and road grade (a) are provided as input to the model, and the driver's model follows during the simulation. At this point it is important to mention that the model applies a forward simulation approach, and the driver is simulated by a PI controller that aims to follow the target velocity from the mission profile input [43].

$$P_{trac} = P_{inertia} + P_{grade} + P_{roll} + P_{aero} \tag{9}$$

$$P_{inertia} = \left(M_{veh}\frac{dv}{dt}\right) v$$

$$P_{grade} = (M_{veh} g sin(a)\,)\, v$$

$$P_{roll} = (c_{roll} M_{veh} cos(a)\,)\, v$$

$$P_{aero} = \left(\frac{1}{2}\rho_{air} A\, C_d\, v^2\right) v$$

A sub-model based on an R-C equivalent circuit was used to simulate the vehicle's Li-ion high voltage battery. For the specific sub-model, the open circuit voltage and ohmic resistance were provided as input, along with the nominal charge and the maximum, minimum and nominal voltage of the vehicle's battery. The core of the simulation model is the energy management strategy that defines powertrain operation. The supervisory control module adopts a rule-based approach that selects the operating point and the power demand of the ICE and the two EMs. This strategy was developed on the basis of observations from the test campaign performed with the vehicle. The complete energy management strategy for the powertrain was devised incorporating user-defined C functions into the vehicle model. The tractive power demand in the case of the vehicle's powertrain architecture considered for this study is covered by the internal combustion engine, and the two electric machines. The energy management strategy selects the operating point of the three components so that the demanded power is fulfilled, and the combustion engine operates with the maximum possible efficiency [44,45]. Consequently, the following conditions may be present:

Pure electric driving or regenerative braking

$$P_{trac} = P_{EM,2} \tag{10}$$

Hybrid driving with $P_{EM,1}$ working as generator with power provided by the ICE

$$P_{trac} = P_{ICE} - P_{EM,1} + P_{EM,2} \tag{11}$$

Hybrid driving with $P_{EM,2}$ working as generator with power provided by the ICE

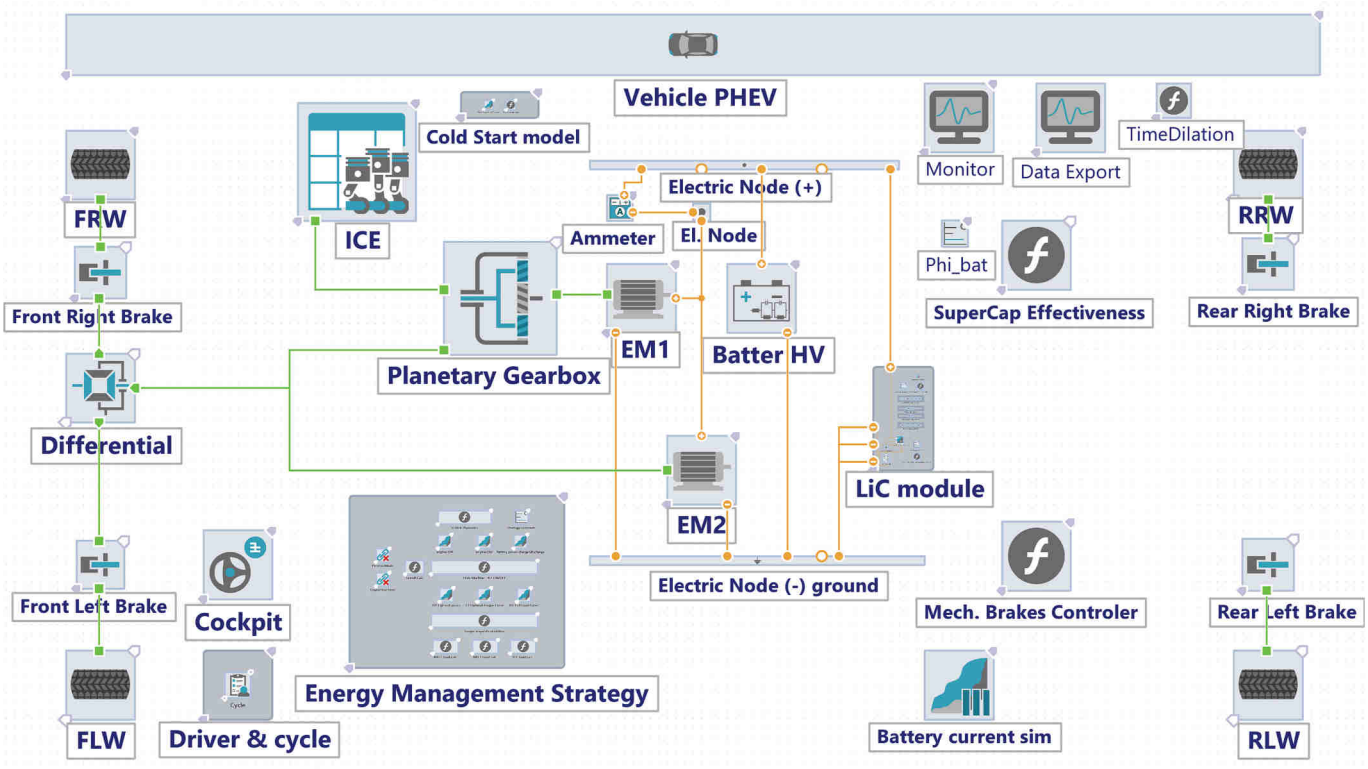

Fig. 12. Vehicle simulation model layout in the AVL CRUISETM M simulation platform.

$$P_{trac} = P_{ICE} + P_{EM,1} - P_{EM,2} \quad (12)$$

Hybrid mode with torque assist from the EMs

$$P_{trac} = P_{ICE} + P_{EM,1} + P_{EM,2} \quad (13)$$

Based on the Eqs. (10), (11), (12) and (13) and the efficiency maps of each component, the operating point is defined and as a result the fuel consumption (for the ICE) and the charge or discharge power of the battery due to the EMs are calculated.

The LiC module was simulated using the ECM presented in the previous subsection. The LiC module was connected to the high voltage electric circuit of the vehicle model using a DC/DC bidirectional power converter integrated into the same model subsystem.

The energy management strategies that defined the LiC module's current demand were implemented as user-defined C functions, like the powertrain's energy management strategy. The required signals were retrieved from the model's data bus and provided as input into the C calculation functions. The output of the calculation functions is the current demand on the side of the DC/DC converter to which the LiC sub-model is connected. In addition, a calculation function was applied to limit the LiC module's current demand. To ensure that the LiC module is not discharged completely, and to avoid overcharge, the current demand was limited or set to zero. The current limit was determined using the voltage of the LiC module, as explained in [41].

As mentioned above, the vehicle model was calibrated using experimental data from a series of cold- and warm-start driving cycles performed in the laboratory. Emissions were measured instantaneously during the tests, whereas aggregate results were obtained through bag analysis. In addition to emissions, OBD signals were measured with reference to engine speed, engine load value, equivalence ratio, high voltage battery state of charge, current and voltage. During laboratory testing, the vehicle was also equipped with an AVL X-ion power analyzer that recorded the current and voltage of the two electric motors. This device was used to record the alternating current and voltage with high frequency while the data acquisition software calculated the electric power of the two electric machines in real time. Power analyzer data was used to study the power flow within the different components of the powertrain. Data from the power analyzer were processed to identify the operation of the electric part of the powertrain. From the measured data it was possible to identify the power of each electric machine. In combination with the fuel consumption measurement and the OBD recording for battery voltage and current and ICE speed it was possible to identify the power split applied during the cycles. This analysis provided the necessary information to understand the vehicle's energy management strategy. The power of the electric motors were two crucial signals, since supervisory control unit introduced in the simulation model was developed on the basis of these measured data. With the recording of electric motors' power it was possible to identify, mainly during CS mode, when the battery was charged or discharged. Additionally, it provided the power demand from the battery or the ICE was allowed to define the power split and the operating point of the engine. Furthermore, it was possible to identify the power demand threshold that leads to the ICE turn-on and engagement.

A second part of the study involved on-road tests using two different vehicles of the same make and model. Details on this case study are presented in previous works by the authors [29,30]. During on-road testing the vehicles were driven over RDE compliant and real-world routes. Emissions were measured using a Portable Emissions Measurement System (PEMS) device, whereas OBD signals were recorded using a logging device. Vehicle position and velocity were also recorded using a Global Positioning System (GPS). The experimental set-up is illustrated in Fig. 13.

Data obtained from the laboratory and real-world testing were also used for model validation of the vehicle simulation model. Emission measurements were used to calculate the fuel consumption using the carbon balance method, while power measurements used to validate power management of the vehicle. It is important to state that the experimental campaign was performed with only the vehicle without the addition of the LiC module. Hence the cases study considered in the current paper used two validated simulation model (the vehicle and the LiC module model).

4. Results and discussion

Three real-world mission profiles (velocity and altitude profile) were used to evaluate the energy management strategies proposed in previous sections. These profiles were acquired through the vehicle experimental set-up described in the previous sections and are considered representative profiles. They include most real-world driving conditions. Details about these profiles in terms of velocity, altitude and driving dynamics are reported in Fig. 14.

The first mission profile (Fig. 14 A – blue solid line) represents normal driving over an RDE-compliant route with limited slope variation. The second mission profile (Fig. 14 A – green solid line) is derived from a real-world test with aggressive driving over an RDE-compliant route. For this profile the driver made frequent abrupt accelerations and decelerations throughout the driving cycle (urban, rural, motorway) while staying within the RDE limits. The influence of the mission profile on plug-in hybrid vehicle operations is also reported in [29].

Although the two mission profiles considered in this study are similar, the main specifications presented in Table 3 highlight the difference in the driving style. For the normal driving style, the average positive acceleration was 0.24 m/s^2, whereas for the aggressive mission

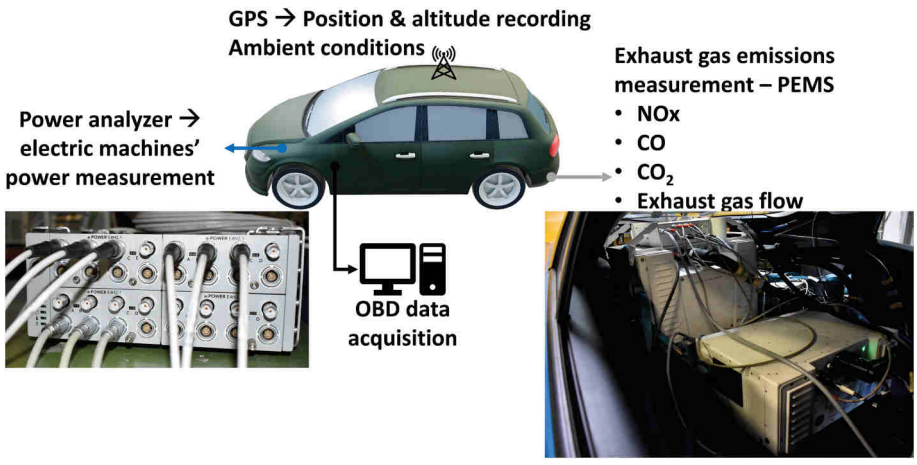

Fig. 13. Schematic of the experimental set-up.

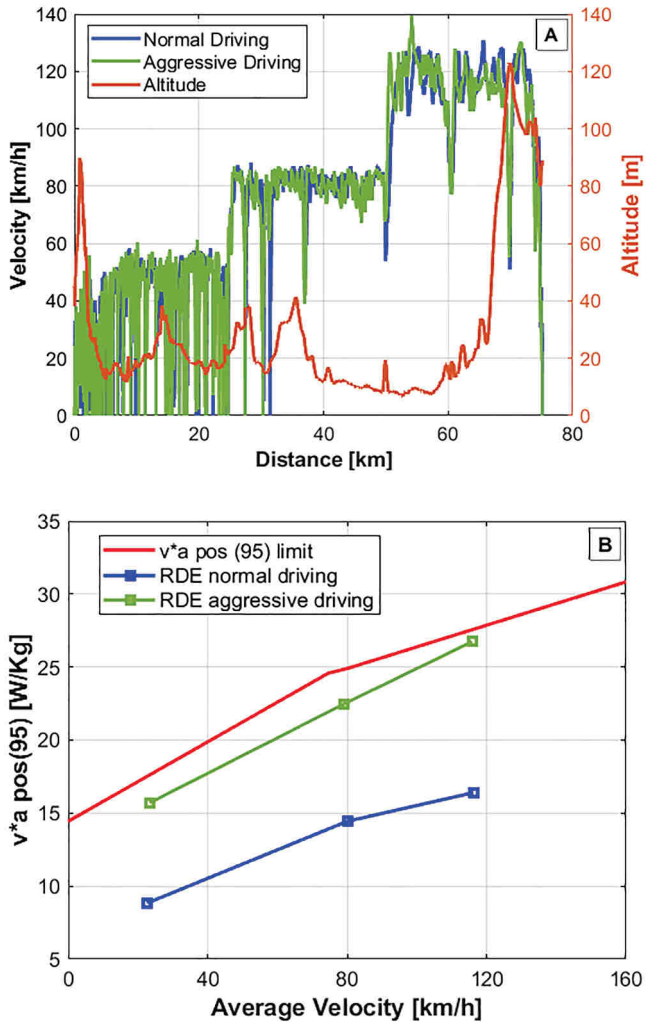

Fig. 14. Mission profiles used for the simulation, (a) RDE -compliant with normal and aggressive driving, (b) driving dynamics of the velocity profiles.

Table 3
Main characteristics of the mission profiles.

	RDE normal driving	RDE aggressive driving
Average velocity (km/h)	44	45
Max. velocity (km/h)	131	139
Average acceleration (m/s2)	0.24	0.34
RPA (m/s2) (Urban/rural/highway)	0.187/0.096/0.106	0.230/0.109/0.145
Urban/rural/highway share (%)	36/35/29	35/35/30
Total trip length (km)	75	75

profile it was 0.34 m/s^2. The aggressiveness of the mission profiles may also be quantified through the 95th percentile of the product v^*a_{pos} *[W/kg]* (velocity: v and positive acceleration: a_{pos}) for urban, rural and motorway driving. The value of the $(v^*a_{pos})_{95th}$ is high when there are frequent rapid accelerations during a trip [46]. Consequently, the higher the v^*a_{pos} value, the more aggressive the driving style This metric was used as an indicator of the driving style and used to characterize the velocity profiles that present aggressive driving and as a result highly transient conditions. Furthermore, a second metric, the relative positive acceleration (RPA), that is calculated from the summation of v^*a_{pos} divided by the total distance, was also introduced to highlight the difference is the driving style. Higher values of RPA indicate that the profile corresponding to the aggressive driving includes more frequent and stronger accelerations than the normal driving style. These metrics are included in the Regulation (EU) 2017/1151 and are used for the validation of the RDE test trip dynamics. For the profiles used, the v^*a_{pos} for urban, rural and motorway is within the limits of RDE regulations; however, values closer to the limit indicate and characterize an aggressive driving style (Fig. 10 B). Similarly, the RPA of the two profiles is also well within the RDE limits. Lastly, for all trips, the share (in terms of kilometers) of urban, rural and motorway driving was well within the acceptable margins of RDE regulations.

The validated Cruise M vehicle/LiC simulation models were used to simulate the behavior and the performance of the vehicle's electric part after the introduction of the LiC module. To that aim, the model was executed for the mission profiles mentioned above. The main goal was to compare the effectiveness of the proposed EMSs for each of the considered mission profiles, starting from different levels of battery SoC. It is important here to state that for all the simulations, the vehicle's driving resistance was kept constant by applying a realistic road load. Furthermore, the additional mass due to the introduction of the LiC module was considered negligible compared to the mass of the vehicle. Hence the simulated mass of the vehicle was also kept constant and was not increased after the introduction of the LiC module. The introduction of the LiC module did not affect primarily the energy management strategy of the vehicle however it intervened at the total power flow in the electric part.

With the implementation of the LiC module, the main goal as described previously was to smoothen the current profile of the high voltage battery. For the simulation cases examined the high voltage battery current showed a reduction in the transient behavior.

As an example, the results of using the *power-based* strategy, with initial SoC at 60% for the normal driving RDE cycle are reported below. The effectiveness index can be determined on the basis of these results so as to compare performance among all the considered EMSs. For the sake of clarity, the analysis focuses on three different parts of the cycle (urban, rural and motorway). The main results, in terms of battery current and velocity versus time, are shown in Fig. 15.

The battery current profiles reveal that use of the LiC module significantly decreased current fluctuations throughout the driving cycle. In particular, there were maximum reductions of 40 *A*, 98 *A* and 100 *A* in peak current values along the urban, rural and motorway sections of the route respectively. From the data analysis it was observed that the introduction of the LiC module had a significant impact during accelerations and decelerations. Peak power during such conditions was mainly covered by the LiC module. High involvement of the LiC module during these conditions can be observed in Fig. 15. Particularly, in Fig. 15 A it can be observed that high voltage battery current during decelerations for the configuration that includes the LiC is always lower than the current of the base configuration. In Fig. 15 B it can be seen that the power demand during the acceleration before 4200 s is mainly covered by the LiC module. Similarly, the acceleration after 5500 s in motorway part (Fig. 15 C) is also covered by the LiC module.

For the considered cycle, the behavior of the LiC module in terms of current and voltage versus time is reported in Fig. 16.

In particular, the LiC module voltage remained within the allowed 96.8–167.2 *V* range throughout the considered operating cycle. Maximum current values of 200 *A* were observed during both charging and discharging operations, with higher fluctuations while driving on the motorway. This is mainly because higher power demands require greater support from the LiC module. For the conditions with current demand that exceeded the 200 A, the high voltage battery was also stressed more due to reduced involvement of the LiC module.

For the EMSs considered above, an *effectiveness* index of 34% was determined for the normal driving RDE cycle with initial SoC at 60%.

The evolution of the state of charge for the LiC module and for the high voltage battery for the example presented in previous graphs is displayed in Fig. 17 with green and grey solid line respectively. The charge of the LiC module shows a high variability throughout the cycle,

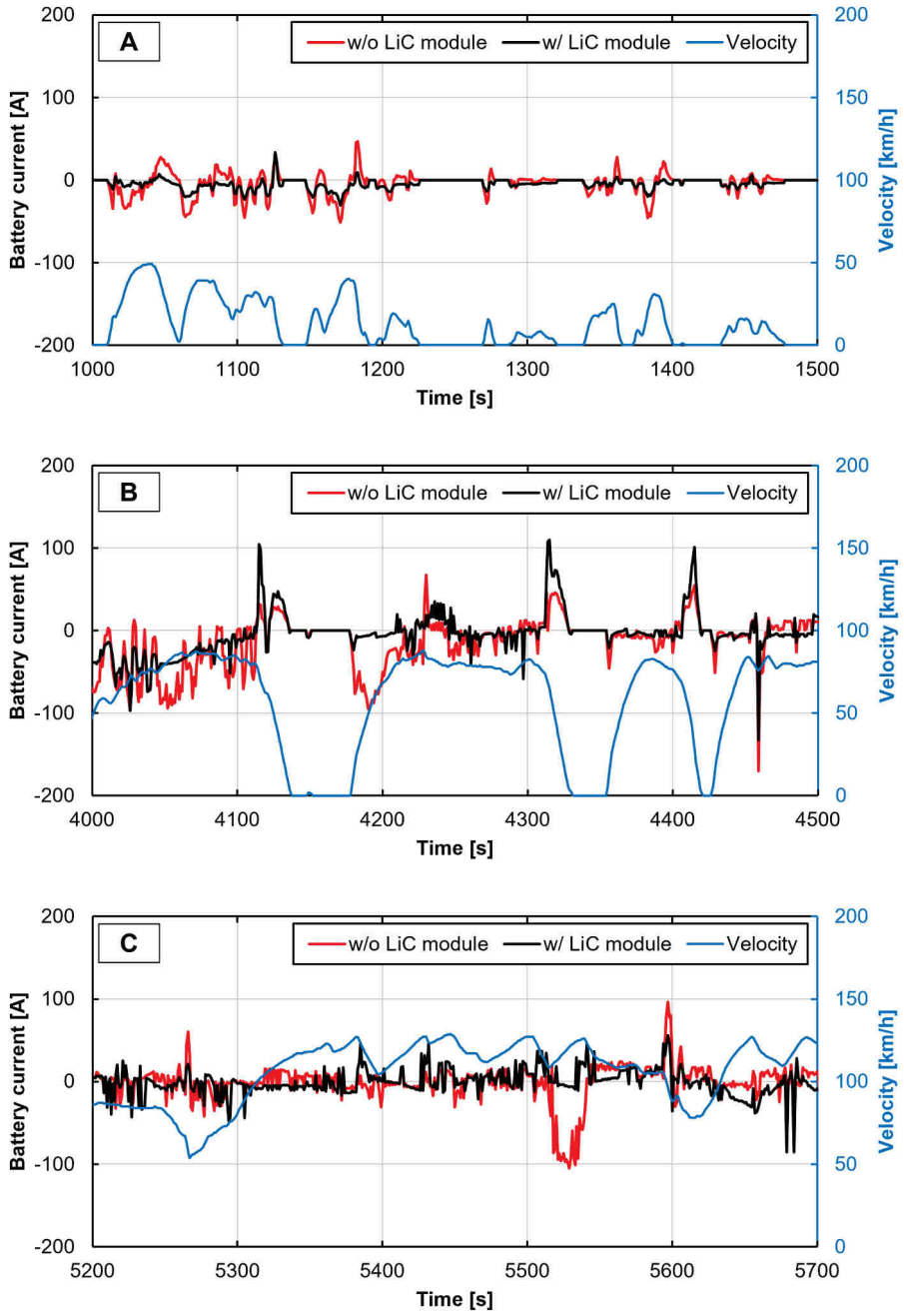

Fig. 15. Battery current with/without the LiC module and velocity versus time for the power-based strategy during the normal driving RDE cycle on urban (A), rural (B) and motorway (C) roads.

mainly due to its nominal capacity. In addition, this frequent fluctuation between 40% and 100% indicates that the LiC module is highly involved at the power flow during vehicle operation. It can be clearly observed when LiC module charging during regenerative braking or when it is discharged when high power demand occurs. In contrast, the high voltage battery indicates as less transient behavior, being constantly discharged until the low SOC threshold is reached and vehicle enters the CS mode. This less transient behavior of the high voltage battery's SOC is mainly due to the nominal capacity but also due to the implementation of the LiC module.

Similar evaluations were performed for the other strategies under different operating conditions. In particular, three levels representing low SoC (15%), medium SoC (60%) and high SoC (85%) were considered. Comparison among EMSs at different initial SoC values was made because, as described in the *Case Study* subsection, power-sharing between the Internal Combustion Engine (ICE) and the electric drives is performed on the basis of the high voltage battery SoC.

Results, in terms of effectiveness, are reported in Fig. 18 for all the considered simulations. This figure clearly shows higher effectiveness values for low initial SoC values. This is mainly because, although these conditions lead to engine activation, lower SoC values entail higher battery current values during both charging and discharging procedures. Under these conditions, the use of the LiC module therefore helps reduce battery peak current demands. A maximum value of 55% effectiveness was reached during the RDE normal driving cycle adopting the *EWMA* strategy. For all considered EMSs there was a slight decrease in effectiveness during aggressive driving conditions. This behavior is ascribed to the fact that such cycles drain the battery pack excessively, while the

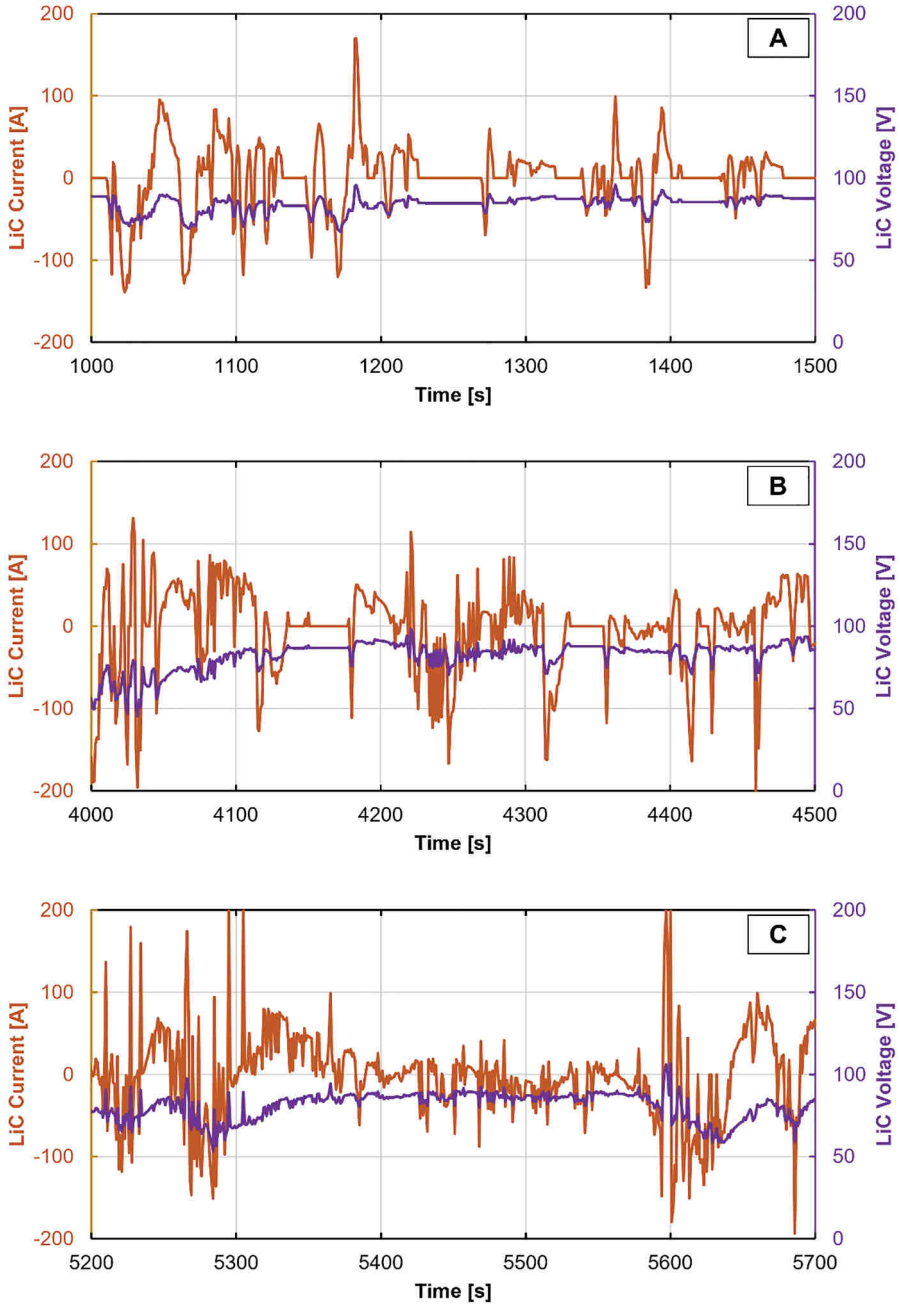

Fig. 16. LiC module current and voltage versus time for the power-based strategy during the normal driving RDE cycle on the urban (A), rural (B) and motorway (C) sections of the route.

current limit of *200 A* limits the support provided by the LiC module. This limit was introduced to avoid extreme discharge or overcharge of the LiC module. However, even under these operating conditions, effectiveness values reached about 40%. Among the strategies studied in this work, both the *power-based* and the *EWMA* strategy yielded higher performance indexes under most of the considered operating conditions. This behavior can be ascribed to their adaptive implementation, which recursively consider the trend of the studied operating cycle. The performance of the *Th* strategy rapidly decreased under power-demanding conditions.

Results amply confirm the advantages of using hybrid energy storage systems supported by proper energy management strategies. There are significant advantages in terms of vehicle battery pack durability: capacitor modules based on LiC technology can be implemented to smooth current fluctuations and peak demands.

5. Conclusion

Three Energy Management Strategies for Hybrid Energy Storage Systems were evaluated through the case study of a commercial C-segment PHEV supplied by a hybrid battery/Lithium-Ion Capacitor storage unit.

Evaluations were carried out using an advanced vehicle simulation platform validated with data obtained through on-board vehicle measurement campaigns. LiC cell model identification and validation procedures were performed through additional experimental activities, which revealed the good fit between the considered simulation model and experimental data from laboratory tests.

A specific measurement campaign was undertaken to acquire RDE driving cycles characterized by different driving styles and dynamics.

The simulation platform allowed easy, rapid optimization and

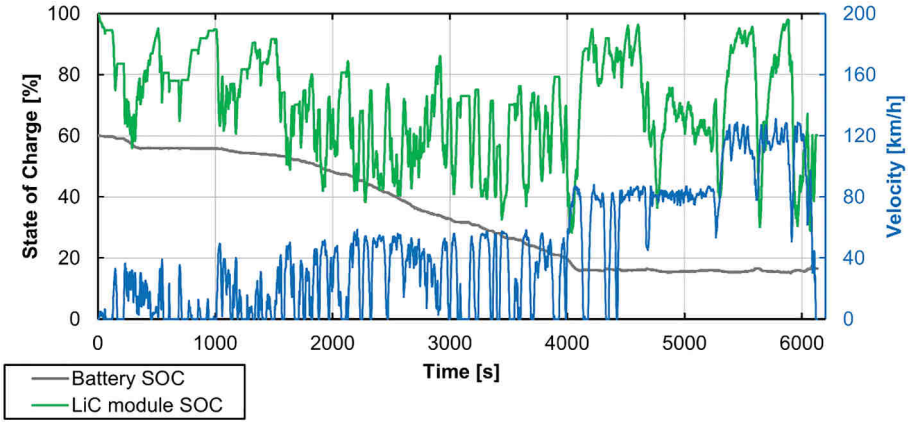

Fig. 17. Battery and LiC Module State of Charge during the normal RDE driving cycle.

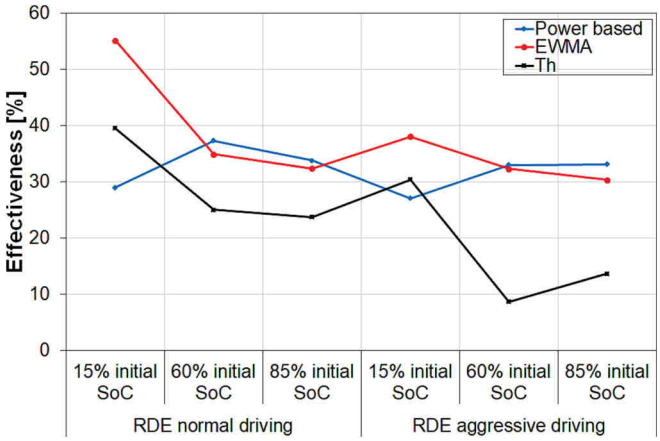

Fig. 18. Effectiveness values for all the simulations.

evaluation of the proposed EMSs, with relevant advantages in terms of the duration and cost of vehicle experimentation.

Results show that the use of HESSs, supported by the implementation of appropriate EMSs, can be considered a good solution for increasing the battery pack's expected cycle life. In addition, LiC technology can be successfully implemented to reduce the impact of this additional storage module in terms of weight and size.

The advantages of the proposed system could pave the way for manufacturers to reconsider the overall storage design (e.g. reducing the battery pack size) of their vehicles on the basis of a cost/benefit analysis that takes into account the specific vehicle mission and expected storage system durability.

CRediT authorship contribution statement

C. Beatrice: Funding acquisition, Conceptualization. **C. Capasso:** Writing – review & editing, Writing – original draft, Validation, Methodology, Formal analysis. **S. Doulgeris:** Writing – original draft, Software, Investigation, Data curation. **Z. Samaras:** Funding acquisition, Conceptualization. **O. Veneri:** Supervision.

Declaration of Competing Interest

The authors declare that they have no known competing financial interests or personal relationships that could have appeared to influence the work reported in this paper.

Data availability

Data will be made available on request.

Acknowledgment

This project received funding from the European Union's Horizon 2020 VISION-xEV Research and Innovation Program under grant agreement No 824314.

References

[1] Krause J, et al. EU road vehicle energy consumption and CO2 emissions by 2050 – Expert-based scenarios. Energy Policy 2020;138:111224. March 2020, https://doi.org/10.1016/j.enpol.2019.111224.
[2] Andersson Ö, Börjesson P. The greenhouse gas emissions of an electrified vehicle combined with renewable fuels: life cycle assessment and policy implications. Apll Energ 2021;289:116621. https://doi.org/10.1016/j.apenergy.2021.116621.
[3] Wood E, Alexander M, Bradley TH. Investigation of battery end-of-life conditions for plug-in hybrid electric vehicles. J Power Sources 2011;196(11):5147–54. https://doi.org/10.1016/j.jpowsour.2011.02.025.
[4] Smith K, Earleywine M, Wood E, Neubauer J, Pesaran A. Comparison of Plug-In Hybrid Electric Vehicle Battery Life Across Geographies and Drive Cycles. in SAE World Congress and Exhibition, April 24-26, 2012, Detroit, Michigan. 2023. https://doi.org/10.4271/2012-01-0666.
[5] Vukajlović N, Milićević D, Dumnić B, Popadić B. Comparative analysis of the supercapacitor influence on lithium battery cycle life in electric vehicle energy storage. J Energy Storage 2020;31:101603. https://doi.org/10.1016/j.est.2020.101603.
[6] Veneri O, Capasso C, Patalano S. Experimental investigation into the effectiveness of a super-capacitor based hybrid energy storage system for urban commercial vehicles. J Appl Energ 2018;227:312–23. https://doi.org/10.1016/j.apenergy.2017.08.086.
[7] Capasso C, Lauria D, Veneri O. Experimental evaluation of model-based control strategies of sodium-nickel chloride battery plus supercapacitor hybrid storage systems for urban electric vehicles. J Appl Energ 2018;228:2478–89. https://doi.org/10.1016/j.apenergy.2018.05.049.
[8] Firouz Y, Omar N, Timmermans JM, Van Den Bossche P, Van Mierlo J. Lithium-ion capacitor–characterization and development of new electrical model. Energy 2018;83:597–613. https://doi.org/10.1016/j.energy.2015.02.069.
[9] Jagadale A, Zhou X, Xiong R, Dubal DP, Xu J, Yang S. Lithium ion capacitors (LICs): development of the materials. Energy Storage Mater 2019;19:314–29. https://doi.org/10.1016/j.ensm.2019.02.031.
[10] Haokun S, Min D, Wanqing W, Qinggong Z, Benhao H. Application of microdiverse carbon materials and loaded binary metals in lithium-ion capacitors. J Energy Storage 2023;60:106550. https://doi.org/10.1016/j.est.2022.106550.
[11] Naseri F, Karimi S, Farjah E, Schaltz E. Supercapacitor management system: a comprehensive review of modeling, estimation, balancing, and protection techniques. Renew Sustain Energy Rev 2022;155:111913. https://doi.org/10.1016/j.rser.2021.111913.
[12] Mohammed AS, Atnaw SM, Salau AO, Eneh JN. Review of optimal sizing and power management strategies for fuel cell/battery/super capacitor hybrid electric vehicles. Energy Rep 2023;9:2213–28. https://doi.org/10.1016/j.egyr.2023.01.042.
[13] Mounica V, Obulesu YP. Hybrid power management strategy with fuel cell, battery, and supercapacitor for fuel economy in hybrid electric vehicle application. ENERGIES 2022;15(12):4185. https://doi.org/10.3390/en15124185.

[14] Azizi I, Radjeai H. A new strategy for battery and supercapacitor energy management for an urban electric vehicle. Elect Eng 2018;100(2):667–76. https://doi.org/10.1007/s00202-017-0535-1.
[15] Song Z, Hofmann H, Li J, Hou J, Han X, Ouyang M. Energy management strategies comparison for electric vehicles with hybrid energy storage system. Appl Energy 2014;134:321–31. https://doi.org/10.1016/j.apenergy.2014.08.035.
[16] Omar N, et al. Electrical double-layer capacitors in hybrid topologies —assessment and evaluation of their performance. Energies 2012;5(11):4533–68. https://doi.org/10.3390/en5114533.
[17] Golchoubian P, Azad NL. Real-time nonlinear model predictive control of a battery–supercapacitor hybrid energy storage system in electric vehicles. IEEE T Veh Technol 2017;66(11):9678–88. https://doi.org/10.1109/TVT.2017.2725307.
[18] Chen H, Xiong R, Lin C, Shen W. Model predictive control based real-time energy management for hybrid energy storage system. Journal of Power and Energy Systems 2021;7(4):862–74. https://doi.org/10.17775/CSEEJPES.2020.02180.
[19] Zhang S, Xiong R, Cao J. Battery durability and longevity based power management for plug-in hybrid electric vehicle with hybrid energy storage system. Appl Energy 2016;179:316–28. https://doi.org/10.1016/j.apenergy.2016.06.153.
[20] Ali M, Ghanbar M, Söffker D. Optimal control of multi-source electric vehicles in real time using advisory dynamic programming. IEEE T Veh Technol 2019;68(11):10394–405. https://doi.org/10.1109/TVT.2019.2941523.
[21] Ali M, Söffker D. Realtime application of progressive optimal search and adaptive dynamic programming in multi-source HEVs. In: Dynamic Systems and Control Conference American Society of Mechanical Engineers. 58288; 2017. https://doi.org/10.1115/DSCC2017-5081. V002T17A003.
[22] Wegmann R, Döge V, Becker J, Sauer DU. Optimized operation of hybrid battery systems for electric vehicles using deterministic and stochastic dynamic programming. J Energy Storage 2017;14:22–38. https://doi.org/10.1016/j.est.2017.09.008.
[23] Mesbahi T, et al. Optimal energy management for a li-ion battery/supercapacitor hybrid energy storage system based on a particle swarm optimization incorporating Nelder–Mead simplex approach. IEEE T Intell Vehicles 2017;2:99–110. https://doi.org/10.1109/TIV.2017.2720464.
[24] Shen J, Khaligh A. A supervisory energy management control strategy in a battery/ultracapacitor hybrid energy storage system. IEEE T Trans Elec 2015;1(3):223–31. https://doi.org/10.1109/TTE.2015.2464690.
[25] Sun L, Feng K, Chapman C, Zhang N. An adaptive power-Split strategy for battery–supercapacitor powertrain—design, simulation, and experiment. IEEE T on power electronics. T Power Electr 2017;32(12):9364–75. https://doi.org/10.1109/TPEL.2017.2653842.
[26] Akar F, Tavlasoglu Y, Vural B. An energy management strategy for a concept battery/ultracapacitor electric vehicle with improved battery life. IEEE T Trans Elec 2017;3:191–200. https://doi.org/10.1109/TTE.2016.2638640.
[27] Pisal PS, Vidyarthi A. An optimal control for power management in super capacitors/battery of electric vehicles using deep neural network. J Power Sources 2022;542:231696. https://doi.org/10.1016/j.jpowsour.2022.231696.
[28] Wang J, Zhou J, ZhaoW.. Deep reinforcement learning based energy management strategy for fuel cell/battery/supercapacitor powered electric vehicle. Green energy and intelligent. Transportation 2022;1(2):100028. https://doi.org/10.1016/j.geits.2022.100028.
[29] Doulgeris S, Toumasatos Z, Prati MV, Beatrice C, Samaras Z. Assessment and design of real world driving cycles targeted to the calibration of vehicles with electrified powertrain. Int J Energ Res 2021;22(12):3503–18. https://doi.org/10.1177/14680874211038729.
[30] Prati MV, Costagliola MA, Guizzo R, Corsetti C, Beatrice C. Emissions and energy consumption of a plug-in hybrid passenger car in real driving emission (RDE) test. Transport Eng 2021;4:100069. https://doi.org/10.1016/j.treng.2021.100069.
[31] Kapadia J, et al. Powersplit or parallel - selecting the right hybrid architecture. Sae Int J Alt Power 2017;6(1):68–76. https://www.jstor.org/stable/26169150.
[32] Castaings A, Lhomme W, Trigui R, Bouscayrol A. Comparison of energy management strategies of a battery/supercapacitors system for electric vehicle under real-time constraints. Appl Energy 2016;2016(163):190–200. https://doi.org/10.1016/j.apenergy.2015.11.020.
[33] Song Z, Hofmann H, Li J, Han X, Zhang C, Ouyang M. A comparison study of different semi-active hybrid energy storage system topologies for electric vehicles. J Power Sources 2015;274:400–11. https://doi.org/10.1016/j.jpowsour.2014.10.061.
[34] Capasso C, Lauria D, Veneri O. Experimental evaluation of model-based control strategies of sodium-nickel chloride battery plus supercapacitor hybrid storage systems for urban electric vehicles. Appl Energy 2018;228:2478–89. https://doi.org/10.1016/j.apenergy.2018.05.049.
[35] Veneri O, Capasso C, Patalano S. Experimental investigation into the effectiveness of a super-capacitor based hybrid energy storage system for urban commercial vehicles. Appl Energy 2018;227:312–23. https://doi.org/10.1016/j.apenergy.2017.08.086.
[36] Song Z, et al. Energy management strategies comparison for electric vehicles with hybrid energy storage system. Appl Energy 2014;134:321–31. https://doi.org/10.1016/j.apenergy.2014.08.035.
[37] Phan DC, Luu NA. Evaluation of exponential moving average application to smooth the power output of wind turbine with different control modes. Int J Elec Comp Eng 2021;11(6):2088–8708. https://doi.org/10.11591/ijece.v11i6.pp4708-4717.
[38] Moumouni Y, Baghzouz Y, Bohem RF. Power “smoothing” of a commercial-size photovoltaic system by an energy storage system. In: 16th International Conference on Harmonics and Quality of Power (ICHQP); 2014. p. 640–4. https://doi.org/10.1109/ICHQP.2014.6842838.
[39] Hossain M, Saha S, Haque ME, Arif MT, Oo A. A parameter extraction method for the Thevenin equivalent circuit model of Li-ion batteries. In: IEEE Industry Applications Society Annual Meeting; 2019. p. 1–7. https://doi.org/10.1109/IAS.2019.8912326.
[40] Locorotondo E, et al. Online identification of thevenin equivalent circuit model parameters and estimation state of charge of lithium-ion batteries. In: IEEE International Conference on Environment and Electrical Engineering and 2018 IEEE Industrial and Commercial Power Systems Europe (EEEIC/I&CPS Europe); 2018. p. 1–6. https://doi.org/10.1109/EEEIC.2018.8493924.
[41] Beatrice C, Capasso C, Doulgeris S, Riccardi M, Samaras Z, Veneri O. Model based evaluation of lithium ion capacitors use and manag.ement for plug-in hybrid vehicles. In: IEEE Vehicle Power and Propulsion Conference (VPPC); 2021. p. 1–7. https://doi.org/10.1109/VPPC53923.2021.9699329.
[42] Hunt G. USABC electric vehicle battery test procedures manual. Washington, DC, USA: United States Department of Energy; 1996.
[43] Onori S, Serrao L, Rizzoni G. Hybrid Electric Vehicles – Energy Management Strategies. Springer briefs in electrical and computer engieering – Control, automation and robotics. 2016. https://doi.org/10.1007/978-1-4471-6781-5.
[44] Kato S, et al. Development of multi stage hybrid system for new Lexus coupe. Sae Int J Altern Powertrains 2017;6:136–44. https://doi.org/10.4271/2017-01-1173.
[45] Ichikawa S, et al. Development of new plug-in hybrid system for compact-class vehicle. Sae Int J Altern Powertrains 2017;6:95–102. https://doi.org/10.4271/2017-01-1163.
[46] Toumasatos Z, et al. The role of the driving dynamics beyond RDE limits and DPF regeneration events on pollutant emissions of a Euro 6d-temp passenger vehicle. J Aerosol Sci 2022;161:105947. https://doi.org/10.1016/j.jaerosci.2021.105947.